Large Conduction Band Energy Offset is Critical for Extracting Electron from Inorganic Perovskite in Efficient Solar Cells

Qiong Wang[1]*, Fengshuo Zu[2], Pietro Caprioglio[3,4], Christian M. Wolff[3], Martin Stolterfoht[3], Meng Li[1,5], Silver-Hamill Turren-Cruz[1], Norbert Koch[2,5,6], Dieter Neher[3], Antonio Abate[1,7,8]*

[1]Young Investigator Group Active Materials and Interfaces for Stable Perovskite Solar Cells, Helmholtz-Zentrum Berlin für Materialien und Energie, Kekuléstraße 5, 12489 Berlin, Germany

[2]Institut für Physik & IRIS Adlershof, Humboldt-Universität zu Berlin, 12489 Berlin, Germany

[3]Institute for Physics and Astronomy, University of Potsdam, Karl-Liebknecht-Straße 24−25, 14476 Potsdam-Golm, Germany

[4]Young Investigator Group Perovskite Tandem Solar Cells, Helmholtz-Zentrum Berlin für Materialien und Energie GmbH, Kekuléstraße 5, 12489 Berlin, Germany

[5]Jiangsu Key Laboratory for Carbon-Based Functional Materials & Devices, Institute of Functional Nano & Soft Materials (FUNSOM), Soochow University, Suzhou 215123, China

[6]Helmholtz-Zentrum Berlin für Materialien und Energie GmbH, Kekuléstraße 5, 12489 Berlin, Germany

[7]Department of Chemical, Materials and Production Engineering, University of Naples Federioco II, Piazzale Tecchio 80, 80125 Fuorigrotta, Naples, Italy.

[8]State Key Laboratory of Photocatalysis on Energy and Environment, Institute of Advanced Energy Materials, Fuzhou University, Fuzhou, Fujian 350002, China

qiong.wang@helmholtz-berlin.de; antonio.abate@helmholtz-berlin.de

Abstract: Charge extraction at the interface of the electron selective contact and the perovskite plays an essential role in photocurrent collection and thereby, the fill factor of solar cells. Here, we studied the charge extraction at the pertinent interface in inorganic perovskite solar cells with two different electron selective contact materials, *i.e.* titanium dioxide (TiO_2) and tin dioxide (SnO_2). We found that the charge extraction between SnO_2 and $CsPbI_{1.8}Br_{1.2}$ perovskite is strongly limited by the low conduction band minimum energy offset of approximately 250 meV. In contrast, TiO_2 has a higher energy offset (400 meV) against the conduction band minimum of $CsPbI_{1.8}Br_{1.2}$ perovskite. This resulted in a superior fill factor up to 78% with a power conversion efficiency of up to 13.3% for inorganic perovskite solar cells with a TiO_2-based electron selective contact. Compared to the mixed organic-inorganic triple cation perovskite ($Cs_{0.05}(FA_{0.83}MA_{0.17})_{0.95}Pb(I_{0.83}Br_{0.17})_3$, where FA is formamidinium, and MA is methylammonium), the inorganic $CsPbI_{1.8}Br_{1.2}$ perovskite demands a much higher conduction

band energy offset for efficient charge extraction. This work provides a clear guideline for the future design and choice of electron selective contacts for inorganic perovskite solar cells.

Keywords: inorganic perovskite, electron selective contact, conduction band energy offset, charge extraction, charge collection

Introduction

Compared to mixed organic/inorganic metal halide perovskites, purely inorganic perovskites, have an extraordinary advantage in terms of thermal stability.[1] Robust thermal stability is critical for passing the accelerated ageing test applied for industrial photovoltaics.[2-4] Until today, pure iodide inorganic perovskite $CsPbI_3$ has the smallest bandgap of ~ 1.7 eV among all caesium lead halides. However, this composition transforms from the cubic phase at temperatures above 310 °C to the delta phase at room temperature[5-7], which represents a thermodynamic stability issue. In contrast, mixed halide inorganic perovskites such as $CsPbI_{3-x}Br_x$ have demonstrated a highly stable cubic or slightly distorted orthorhombic phase at room temperature in an inert atmosphere, *i.e.* nitrogen-filled glove box.[8, 9] Solar cells with compositions of $CsPbI_{3-x}Br_x$ perovskite thus exhibit great potential. In recent years, a power conversion efficiency (PCE) of over 16% has been reported for $CsPbI_2Br$ perovskite.[10, 11] However, the photocurrent is likely overestimated in many works[10-13] because the maximum short-circuit photocurrent (J_{sc}) at a bandgap of 1.9 eV for $CsPbI_2Br$[14-16] is 16.97 mA cm^{-2}, based on the Shockley-Queisser equation for single-junction solar cells, considering only radiative recombination.[17] In reality, we calculated the maximum J_{sc} of 16.16 mA cm^{-2} at an external quantum efficiency (EQE) of up to 96% above the bandgap (**Figure S1**). On the other hand, the reported open-circuit voltage (V_{oc}) of $CsPbI_2Br$ inorganic perovskite solar cells of less than 1.25 V[15, 18, 19] is generally much lower than the radiative V_{oc} limit of ~1.589 V[17]. Therefore, to achieve higher efficiency in inorganic perovskite solar cells, we need a higher V_{oc} by reducing the non-radiative recombination at the interfaces with the perovskite film and reduced defects in its bulk.[13]

Many recent works on $Cs_{0.05}(FA_{0.83}MA_{0.17})_{0.95}Pb(I_{0.83}Br_{0.17})_3$ triple cation perovskite[20] (referred as CsFAMA in the following) and methylammonium lead trihalide[21-23] ($MAPbX_3$, X = I, Br, Cl) demonstrated that the energy levels of electron and hole selective contact have a significant influence on the non-radiative recombination at the interface.[24, 25] In general, small energy offset against the valence band maximum (VBM) of the perovskite, e.g. with poly[bis(4-phenyl)(2,4,6-trimethylphenyl)amine] (PTAA), results in a high V_{oc}, whereas poly(2,3-dihydrothieno-1,4-dioxin)-poly(styrenesulfonate) (PEDOT:PSS) with a large energy offset features a low V_{oc}.[20] Similarly, a small conduction band minimum (CBM) energy offset with electron selective contacts is beneficial for a high V_{oc} as well. In the case of TiO_2 and SnO_2, two commonly used inorganic electron selective contacts (ESCs), the latter allows a higher V_{oc} than TiO_2-based solar cells. Consequently, higher efficiency is achieved in SnO_2-based solar cells.[20] Many works have further demonstrated the superior performance of SnO_2 originated from its

high conductivity[26] and photo-stability against UV light[27, 28]. For example, Jiang *et al.*[29] deposited SnO_2 from a SnO_2 nanoparticle suspension, followed by annealing on a hot plate at the temperature of 150 °C, and achieved an efficiency of 23% for formamidinium lead triiodide perovskite solar cells. Correa Baena et al.[30] reported a maximum V_{oc} of 1.214 V for CsFAMA-triple cation perovskite solar cells using SnO_2 based ESC prepared by chemical bath deposition. Tavakoli *et al.*[31] prepared SnO_2 from tin chloride dissolved in isopropanol and deposited it on top of TiO_2 to form a double-layered ESCs. They reported a significant increase in V_{oc} and fill factor (FF) of their devices.

Here, we employed TiO_2 and SnO_2 as the ESCs for our inorganic perovskite solar cells with $CsPbI_{1.8}Br_{1.2}$ as the light absorber. $CsPbI_{1.8}Br_{1.2}$ is selected here because we found that $CsPbI_{1.8}Br_{1.2}$ perovskite exhibits robust phase stability compared to $CsPbI_2Br$ perovskite[32]. In particular, we studied the charge extraction and interface recombination in inorganic perovskite solar cells using steady-state photoluminescence and time-resolved photoluminescence. We found that, in line with our previous work[20], SnO_2 exhibits slower interface recombination compared to that of TiO_2. A substantially long non-radiative recombination lifetime of approximately 60 ns is extracted from a FTO/SnO_2/$CsPbI_{1.8}Br_{1.2}$ film, in comparison to around 10 ns for FTO/TiO_2/$CsPbI_{1.8}Br_{1.2}$ stack. As further revealed from ultraviolet photoelectron spectroscopy measurements, SnO_2 has a deeper CBM against the vacuum level and correspondingly smaller energy offset to the perovskite as compared to TiO_2. Although a higher V_{oc} was achieved with SnO_2, the fill factor was worse. This work reveals that a higher CBM energy offset, of over 250 meV is required to provide enough driving force for charge extraction for inorganic perovskite solar cells. Thus, this work will greatly contribute to the future design of ESCs for use in inorganic perovskite solar cells.

Results and discussion

The details regarding the preparation of TiO_2 and SnO_2 contacts and deposition of $CsPbI_{1.8}Br_{1.2}$ are given in the experimental section (see SI). It should be noted that here we adopted the double-layered structure for SnO_2 contacts, as reported in Tavakoli's work[31]. This is because a single SnO_2 compact layer deposited from the sol-gel method frequently resulted in up to 90% shunted devices. By depositing a SnO_2 compact layer on top of a compact TiO_2 (c-TiO_2, prepared from spray-pyrolysis), the percentage of shunted devices is significantly reduced to less than 5%. The reference TiO_2 contact adopts the classic architecture with mesoporous TiO_2 (m-TiO_2) deposited on top of c-TiO_2 covered fluorine-doped tin oxide (FTO). **Figure 1a** illustrates the scheme of the configuration of the studied solar cells with a double-layer

structured ESCs. In the case of SnO_2-ESC based solar cells, the thin SnO_2 layer of less than 50 nm takes the place of a mesoporous TiO_2 layer of around 150 nm. Figures 1b and 1c present cross-section scanning electron microscopy (SEM) images of $CsPbI_{1.8}Br_{1.2}$ deposited on SnO_2-ESC and TiO_2-ESC, respectively. In both cases, the $CsPbI_{1.8}Br_{1.2}$ film has a thickness of approximately 500 nm. The features of m-TiO_2 deposited on top of c-TiO_2 on FTO can be seen in Figure 1c, while the double-layered SnO_2/c-TiO_2 on FTO can also be identified in Figure 1b. Figures 1d and 1e present the surface morphology of $CsPbI_{1.8}Br_{1.2}$ perovskite deposited on SnO_2-ESC and TiO_2-ESC. We can see that both contacts support a compact $CsPbI_{1.8}Br_{1.2}$ perovskite film with similar morphological features.

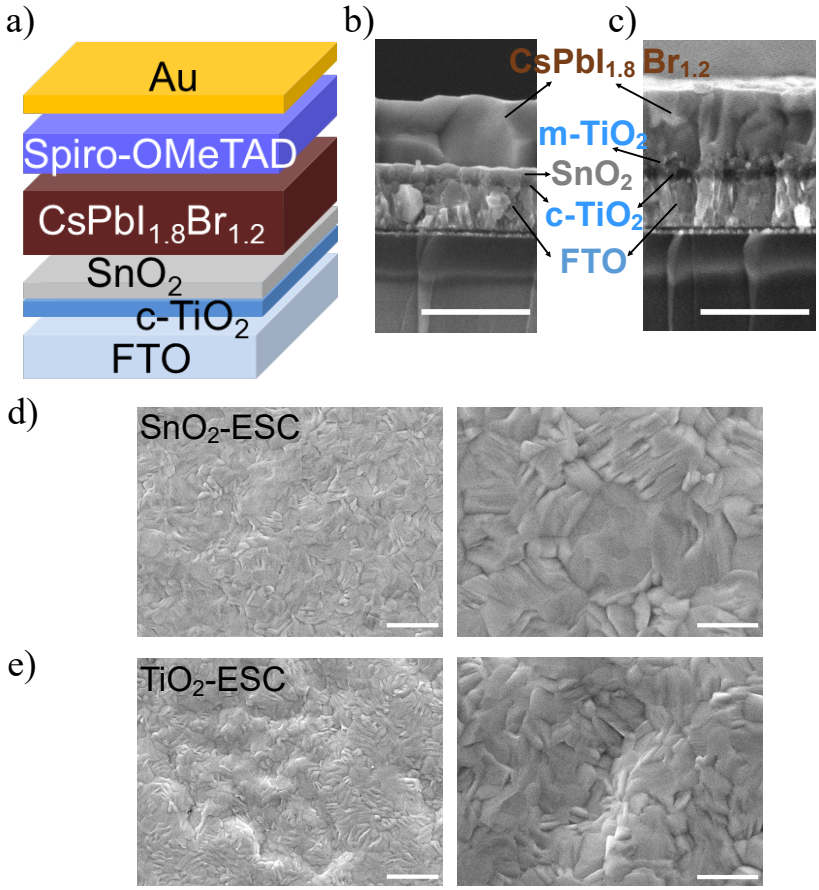

Figure 1. a) Scheme of the structure of inorganic perovskite solar cells using SnO_2/c-TiO_2 double-layered ESCs. Cross-section SEM images of $CsPbI_{1.8}Br_{1.2}$ perovskite deposited on b) SnO_2 and c) TiO_2 covered c-TiO_2/FTO (scale bar: 800 nm). Surface morphology of $CsPbI_{1.8}Br_{1.2}$ perovskite deposited on d) SnO_2 and e) TiO_2 covered c-TiO_2/FTO with low magnification (left panel, scale bar: 2 µm) and high magnification (right panel, scale bar: 800 nm).

Figure 2a reveals that $CsPbI_{1.8}Br_{1.2}$ deposited on TiO_2 and SnO_2 contacts has essentially the same optical bandgap of 1.93 eV. It should be noted that for the UV-Vis absorption measurements and the later-mentioned photoluminescence measurements, which were

conducted in air, the samples were encapsulated with a thin microscopic slide as the cover glass to avoid the permeation of moisture during the measurements. We found that the encapsulation is very critical for these measurements, because without encapsulation $CsPbI_{1.8}Br_{1.2}$ films quickly decomposed into yellow lead iodide. This decomposition process is predominantly triggered by the air humidity that is influenced by weather and season. Solar cells made out of this inorganic perovskite are stored in a dry airbox with constant dry airflow and relative humidity of lower than 0.3%.

Figure 2b reveals the absolute photoluminescence (PL) spectra of $CsPbI_{1.8}Br_{1.2}$ films deposited on bare glass (black line), as well as SnO_2 (red line) and m-TiO_2 (blue line) on c-TiO_2/FTO, respectively. It gives an optical bandgap of around 1.89 eV for $CsPbI_{1.8}Br_{1.2}$ perovskite/glass. A slight shift to the higher energy for $CsPbI_{1.8}Br_{1.2}$ deposited on the contacts is observed, compared to the glass substrate. The reason behind the shift is currently unknown. Importantly, $CsPbI_{1.8}Br_{1.2}$ films deposited on both contacts (SnO_2 and m-TiO_2) exhibit a distinct decrease in photoluminescence quantum yield (PLQY). This demonstrates that both SnO_2 and TiO_2 transport layers introduce significant interface recombination at the perovskite interface or bring additional non-radiative recombination within the transport layer, reducing the amount of free carriers able to recombine radiatively in the perovskite bulk, as previously observed.[20] Moreover, the SnO_2 contact resulted in a less quenched PL signal compared to TiO_2, in line with the previous report on CsFAMA-triple cation perovskite with a smaller bandgap.[20] This trend indicates slower interface recombination at the SnO_2 interface compared to that of TiO_2, or that the charge extraction from the perovskite to the TiO_2 layer is faster which accelerates the overall non-radiative recombination of charges at the interface or within the ESC itself.[33] The maximum quasi-fermi level splitting (QFLS) is calculated from the absolute PLQY following previous works[20, 34], and it is presented in Figure 2c. Details of the calculation can be found in SI (**Figure S2**). Accordingly, with the PLQY values, the QFLS of the different samples illustrates that $CsPbI_{1.8}Br_{1.2}$ deposited on glass features the highest QFLS (1.365 eV), followed by SnO_2-ESC (1.343 eV) and TiO_2-ESC (1.317 eV). As we discuss further below, the trend in QFLS matches well with the trend in V_{oc} of solar cells based on these two contacts, with SnO_2-ESC based solar cells holding a higher V_{oc} than that of TiO_2-ESC. Figure 2d illustrates the time-resolved PL (trPL) measurements. By fitting the PL decay curve with a mono-exponential equation, we calculated that a longer non-radiative recombination lifetime (60 ns) is extracted for $CsPbI_{1.8}Br_{1.2}/SnO_2$ than that of $CsPbI_{1.8}Br_{1.2}/TiO_2$ (10 ns). Therefore, the trPL measurements agree well with the PLQY measurements, confirming slower interface recombination at the interface $CsPbI_{1.8}Br_{1.2}/SnO_2$-ESC.

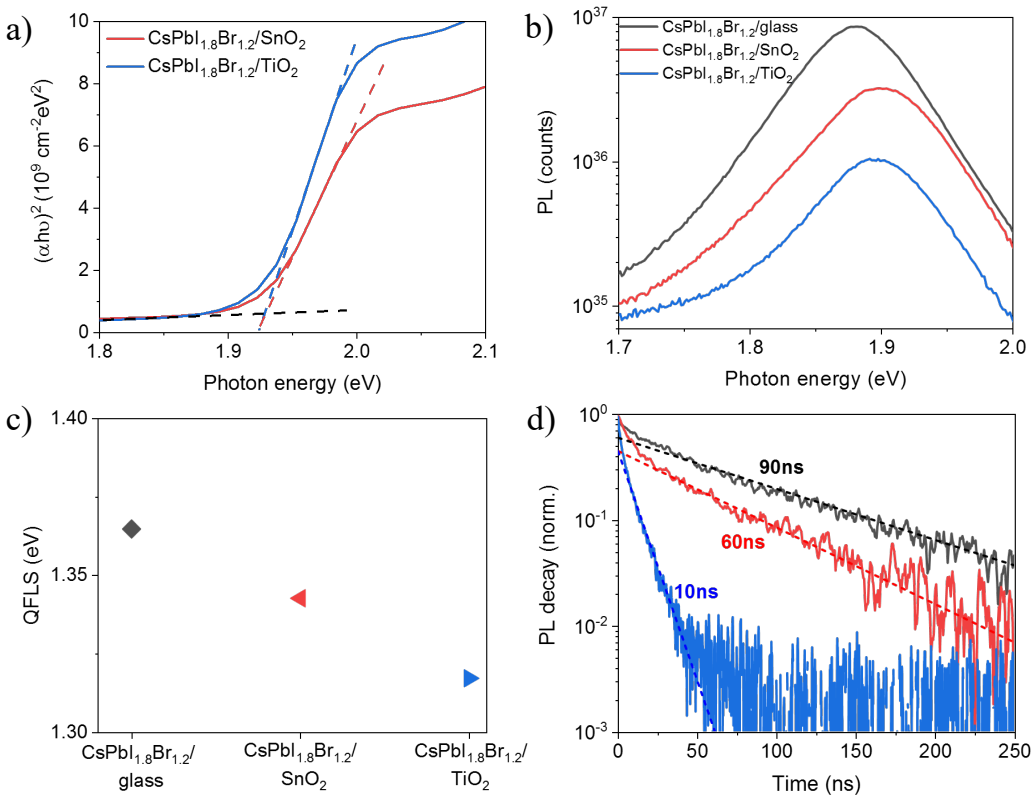

Figure 2. a) Tauc plots of SnO_2-ESC/$CsPbI_{1.8}Br_{1.2}$- (red line) and TiO_2-ESC/$CsPbI_{1.8}Br_{1.2}$- (blue line). b) Absolute PL, c) Quasi Fermi Level Splitting (QFLS), and d) time-resolved PL (trPL) of $CsPbI_{1.8}Br_{1.2}$ deposited on non-conductive glass (black line), SnO_2 (red line) and TiO_2 (blue line) covered FTO/c-TiO_2.

The above PL analysis would suggest that solar cells with compositions of SnO_2-ESC/$CsPbI_{1.8}Br_{1.2}$ would result in a better open-circuit voltage and hence potentially better photovoltaic performance (than that of TiO_2-ESC/$CsPbI_{1.8}Br_{1.2}$). With this expectation in mind, we fabricated inorganic perovskite solar cells using 2,2',7,7'-tetrakis-(N,N-di-*p*-methoxyphenyl-amine)-9,9'-spirobifluorene (spiro-OMeTAD) as the hole selective contact. It should be noted that the "oxygen soaking"[35, 36] of spiro-OMeTAD was conducted by storing the devices overnight in a dry airbox with a very low relative humidity of less than 0.3%. **Figure 3a** displays the *J-V* curve of solar cells based on SnO_2 and TiO_2 contacts for $CsPbI_{1.8}Br_{1.2}$ inorganic perovskite. In agreement with Figure 2c, a higher V_{oc} of 1.294 V is achieved with SnO_2-ESC based solar cells than 1.209 V for that of TiO_2. However, we observed a much lower FF and a smaller J_{sc} for SnO_2-ESC based solar cells. Overall, SnO_2-ESC based inorganic perovskite solar cells result in a much worse photovoltaic performance compared to TiO_2-ESC based inorganic perovskite solar cells. **Table S1** summarises the detailed photovoltaic parameters of J_{sc}, V_{oc} and FF. Figure 3b illustrates the external quantum efficiency (EQE) measurement of the solar cells. It evidences that TiO_2-ESC based inorganic perovskite solar

cells exhibit a high EQE value of approximately 85% over a broad wavelength range. However, SnO_2-ESC based inorganic perovskite solar cells have a much lower EQE value of below 80% for all the wavelength range. This characteristic suggests that there is a big issue in charge extraction in SnO_2-ESC based inorganic perovskite solar cells. This trend is observed in over 12 solar cells. Figures 3c-f summarise box charts of PCE, V_{oc}, J_{sc} and FF. Interestingly, solar cells based on SnO_2-ESC exhibit on average a 100 mV higher V_{oc} than TiO_2-ESC based inorganic perovskite solar cells, yet a 1 mA cm^{-2} lower J_{sc} and an almost 20% lower FF than that of TiO_2-ESC based inorganic perovskite solar cells.

In recent work,[14] we found the first annealing step temperature in a three-step annealing procedure of $CsPbI_{1.8}Br_{1.2}$ inorganic perovskite can significantly influence the charge extraction, indicative of a poor FF and a low EQE. Optimisation of the first annealing step temperature for TiO_2-ESC based inorganic perovskite solar cells resulted in a PCE of 13.3% with a FF up to 78% (**Figure S3**). Similar optimisation of the first annealing step temperature of the inorganic perovskite was conducted on SnO_2-ESC. The distribution of J_{sc} and FF in SnO_2-based solar cells is summarised in Figures 3g-h, with box charts of PCE and V_{oc} summarised in **Figure S4**. It shows a gradual increase in J_{sc} as the first annealing step temperature of $CsPbI_{1.8}Br_{1.2}$ increases, but the FF is generally low at the level of 50%. Figure 3i summarises the EQE response of SnO_2-based solar cells with $CsPbI_{1.8}Br_{1.2}$ annealed at different temperatures ranging from 45 °C to 65 °C with an interval of 5 °C. It displays that the EQE is slightly increased at the wavelength spanning from 350 to 550 nm as the temperature goes up. However, it is generally low (below 80%). It should be noted that a further increase in the temperature does not lead to higher performance in solar cells because of poor morphology of the perovskite film that was processed anti-solvent-free. Overall, it implies that the poor charge extraction is not likely due to the poor crystallisation of the inorganic perovskite, as we studied a wide range of first annealing step temperatures that are found to be crucial for the management of phase purities and crystal orientation.[14] Accordingly, bulk defects in the inorganic perovskite are expected not to play a significant role here. Rather, the energy level alignment at the interface may be the cause of the poor charge extraction in case of SnO_2-based $CsPbI_{1.8}Br_{1.2}$ cells. It is worth noting that by applying a shallow mask during the *J-V* measurements, our J_{sc} given in Figure 3g matches very well with the integrated J_{sc} from EQE (Figure 3i).

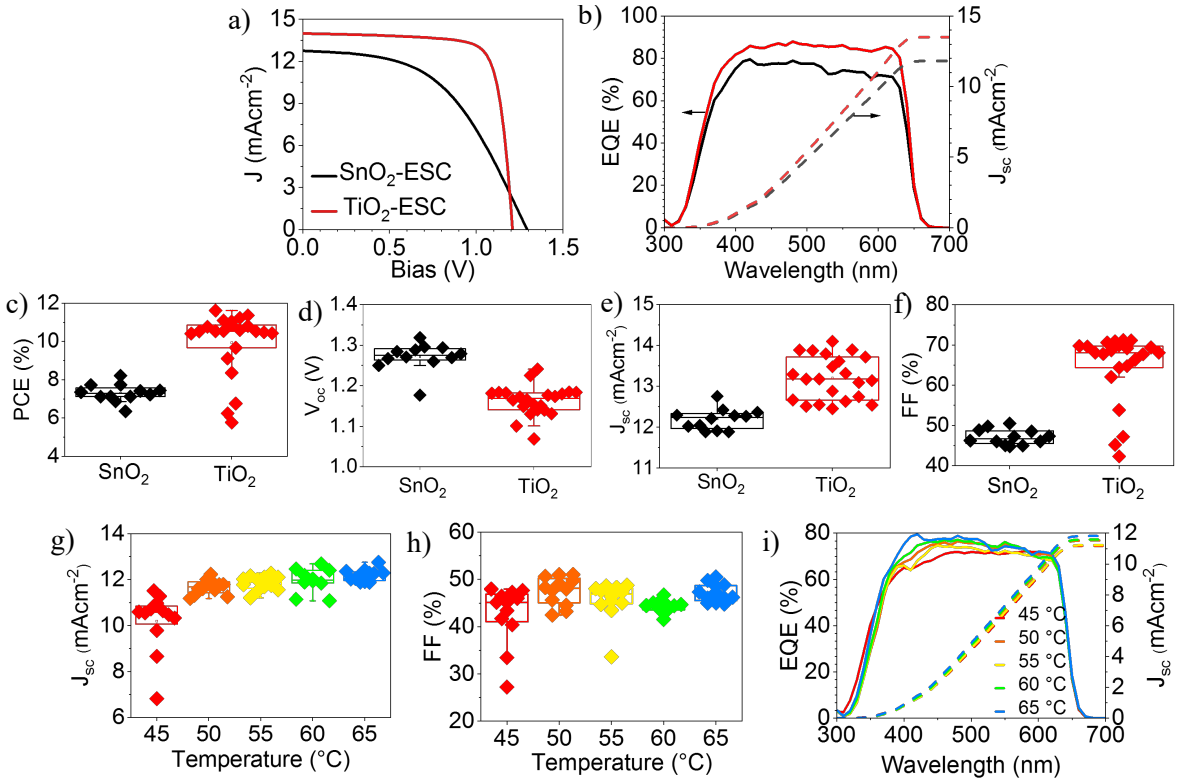

Figure 3. a) *J-V* curve, b) EQE spectra, and box chart of photovoltaic parameters (c: PCE (%), d: V_{oc} (*V*), e: J_{sc} (mAcm^{-2}), f: FF (%)) of the solar cells based on SnO_2 (black line) and TiO_2 (red line) for $CsPbI_{1.8}Br_{1.2}$ inorganic perovskite. Box chart of g) J_{sc} (mA cm^{-2}) and h) FF (%) and i) EQE spectra for inorganic perovskite solar cells based on SnO_2-ESC with $CsPbI_{1.8}Br_{1.2}$ inorganic perovskite annealed at a range of temperatures from 45 °C to 65 °C with an interval of 5 °C. *J-V* curves were measured with a scan rate of 200 mV/s and a shallow mask with an area of 0.1 cm^2.

To unravel the energy level alignment at the interfaces, we conducted ultraviolet photoelectron spectroscopy (UPS) measurements of SnO_2-ESC and TiO_2-ESC with and without $CsPbI_{1.8}Br_{1.2}$ thin films. Moreover, we investigated a CsFAMA-triple cation perovskite on both contacts as reference. The photovoltaic performance of CsFAMA perovskite on these two contacts is given in **Figure S5**. It illustrates that SnO_2-ESC based solar cells exhibit a similar efficiency as those with TiO_2-ESC with an average efficiency of around 16.5%. Similar to inorganic perovskite solar cells, the triple cation perovskite solar cells also achieved a higher V_{oc} (1.157 V) with SnO_2-ESC than that of TiO_2-ESC (1.075 V). This trend agrees with previous work.[20,31, 37]

Figure 4a presents the secondary electron cut-off of all samples (left panel), from which the sample work function (WF) is obtained. It exhibits that SnO_2-ESC has a higher work function of 4.26 eV than TiO_2-ESC of 3.58 eV, in agreement with the previous report.[22] Moreover, for both inorganic perovskite and triple cation perovskite, the work functions are very similar on both contacts. The valence band spectra are given in the middle panel of Figure 4a on a linear

intensity scale, and a zoomed-in spectral region on a logarithmic intensity scale is given in the right panel. The position of the VBM is determined by extrapolation of the leading edge on a logarithmic photoelectron intensity scale to obtain a right band edge.[38, 39] The CBM is calculated from the measured VBM by adding the optical gap of the material with the assumption that the exciton binding energy is negligible at room temperature. The optical gap of SnO_2 and TiO_2 of 3.6 eV and 3.2 eV were measured and given in **Figure S6**. The optical gap of $CsPbI_{1.8}Br_{1.2}$ was determined as 1.93 eV (Figure 2a) while the optical gap of CsFAMA perovskite of 1.61 eV is taken from the steady-state PL spectra (**Figure S7**).

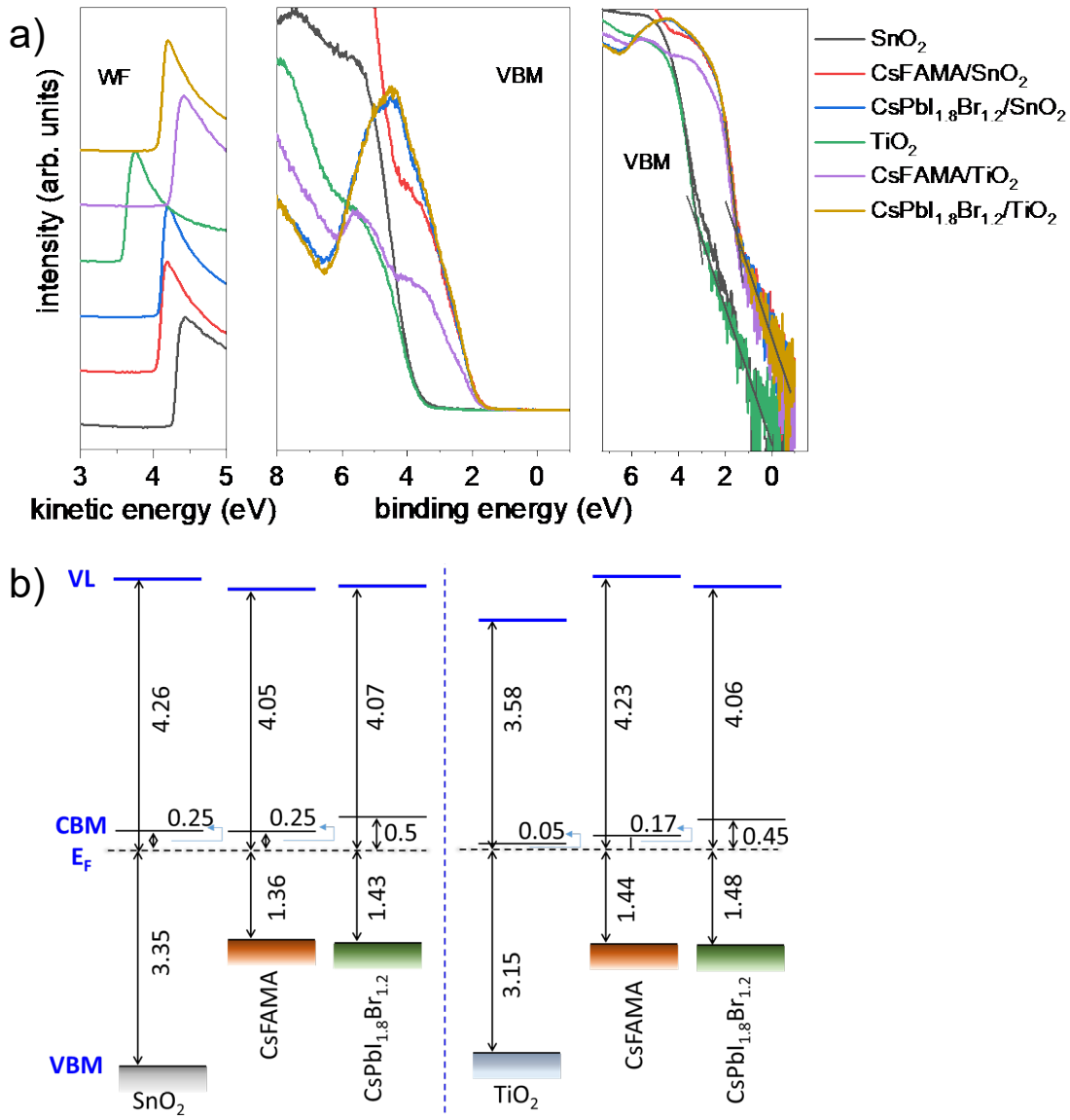

Figure 4. a) Secondary electron cut-off (left panel), valence spectra (middle panel), and zoomed valence spectra on logarithmic intensity scale (right panel) of SnO_2-ESC (black line), CsFAMA/SnO_2-ESC (red line) and $CsPbI_{1.8}Br_{1.2}$/SnO_2-ESC (blue line), TiO_2-ESC (green line), CsFAMA/TiO_2-ESC (pink line) and $CsPbI_{1.8}Br_{1.2}$/SnO_2-ESC (orange line). (b) Schematic energy-level diagram of SnO_2-ESC, TiO_2-ESC, CsFAMA and $CsPbI_{1.8}Br_{1.2}$ relative to E_F.

Figure 4b illustrates the energy level alignment between the contacts and the perovskites. It displays that m-TiO_2 has its CBM very close to the Fermi level (E_F), only 50 meV distance. It should be noted that we used lithium bis(trifluoromethanesulfonyl)imide-doped m-TiO_2 as described in the experimental section (see SI). The reason for doping m-TiO_2 with the lithium salt is to enhance its electron conductivity to reduce the transport resistance on the one hand. On the other hand, to strengthen electron extraction.[40] Though SnO_2 was deposited from its sol-gel solution without any dopant, it presents a high electron conductivity intrinsically,[28, 37, 41] with CBM only 250 meV away from the E_F. Notably, both $CsPbI_{1.8}Br_{1.2}$ and CsFAMA perovskites exhibit an *n*-type character at the surface that is accessible to UPS as the E_F is found to be very close to their CBM. It is noted that in this study, we did not observe any shifts in perovskite energy levels when performing surface photovoltage measurements, indicating a flat band condition through perovskite layers,[20, 39] as illustrated in Figure 4b.

More specifically, in the case of SnO_2-ESC contact, the CBM of CsFAMA perovskite is located at the same position as that of contact, which agrees with a previous report.[37] In comparison, the energy offset between TiO_2-ESC and CsFAMA is around 120 meV. Since both contacts lead to a decent efficiency in solar cells, one concludes that both SnO_2-ESC and TiO_2-ESC can extract electrons efficiently from CsFAMA perovskite and the driving force required for electron extraction from CsFAMA perovskite can be very small or even negligible. In case of the $CsPbI_{1.8}Br_{1.2}$ perovskite, the CBM offsets are 250 meV and 400 meV for SnO_2-ESC and TiO_2-ESC, respectively. Based on the above discussion of the photovoltaic performance of inorganic perovskite solar cells, it is reasonable to conclude that the reason for the poor electron extraction by SnO_2-ESC from $CsPbI_{1.8}Br_{1.2}$ is the small CBM energy offset. Based on our data, we believe that $CsPbI_{1.8}Br_{1.2}$ requires a much higher energy offset, of over 250 meV, for efficient electron extraction. Our conclusion is supported by one recent work from Xu *et al.*[13] who prepared SnO_2 nanoparticles from its colloid solution and used it as ESC for $CsPbI_2Br$, where they measured the CBM energy offset of 300 meV and thus reported a beautiful FF of 75.5% for their solar cells.

The difference between CsFAMA and $CsPbI_{1.8}Br_{1.2}$ perovskites in terms of charge extraction may come from the relatively higher exciton binding energy of the inorganic perovskite. Yang *et al* studied the exciton binding energy of both organic and inorganic perovskites.[42-44] They found that $CsPbI_2Br$ exhibits a value of 22 ± 3 meV that is much higher than the exciton binding energy of 12 ± 3 meV for tetragonal phase $MAPbI_3$ and 13 ± 2 meV for CsFAMA perovskite. Considering the thermal energy at room temperature of ca. 26 meV, both $MAPbI_3$ and CsFAMA perovskites exhibit a non-excitonic behaviour at room temperature. Therefore, even at small

energy offset at the interface between CsFAMA and electron selective contacts, electrons can still efficiently flow from the conduction band of CsFAMA perovskite to that of SnO_2-ESC. However, inorganic perovskites with mixed halides have an exciton binding energy highly close to the thermal energy, indicating that a higher energy offset is required as the driving force for the efficient collection of electrons. Also, compared to inorganic perovskites that exhibit ultrafast (< 0.6 ps) hot-carrier relaxation dynamics,[45] organic-inorganic perovskites were reported to have a slower carrier relaxation time of up to 100 ps,[46-48] which makes the extraction of hot carriers from CsFAMA perovskite even possible. Therefore, it would be fascinating, as next step, to investigate the transient absorption spectra of the system of CsFAMA deposited on SnO_2-ESC to examine whether or not there is any hot carrier extraction happened at the interface.

Conclusion

We studied two electron selective contacts, *i.e.* SnO_2 and TiO_2, for $CsPbI_{1.8}Br_{1.2}$ inorganic perovskite solar cells. Though there is no detrimental energy barrier for both contact materials, $CsPbI_{1.8}Br_{1.2}$ is found to demand a much higher conduction band minimum energy offset to drive efficient electron extraction compared to the CsFAMA triple cation perovskite. Based on UPS data, an energy offset of over 250 meV is needed for efficient charge extraction from $CsPbI_{1.8}Br_{1.2}$. The difference between CsFAMA and $CsPbI_{1.8}Br_{1.2}$ perovskites in terms of charge extraction may come from the relatively higher exciton binding energy of the inorganic perovskite. These results guide the future design and selection of electron transport materials to be used in inorganic perovskite solar cells. Energy level adjustment *via* doping of electron transport materials[49-51] or adopting the form of nanoparticles[13, 28, 52] or tuning of the conduction band energy of inorganic perovskite *via* supramolecular approaches[53, 54] would be fascinating routes to explore for improving charge extraction at the interface of contacts and inorganic perovskites.

Acknowledgement

The authors acknowledge the funding by the DFG (SPP2196). M.S. acknowledges the DFG (423749265). P.G. acknowledges financial support by the HyPerCells, a joint graduate school of Potsdam University and the HZB. Q.W. appreciated the kind assistance from Mrs. Klimm Carola for the SEM measurements.

Author contribution

Q.W. designed the experiment, drafted the manuscript, fabricated and characterised the solar cells and prepared the samples for the measurements. F.S.Z conducted and contributed to the data analysis of the UPS measurements for the work. P.C., C.M.W., M.S. conduced and contributed to the data analysis of the PL measurements for this work. M. L. and S.-H. T.C. provided useful discussion during the conduction of the project. D.N, N.K. and A.A provided valuable inputs on the overall data discussion and manuscript revision. All authors discussed the results and provided feedback on the manuscript.

References

1. Q. Wang, N. Phung, D. Di Girolamo, P. Vivo and A. Abate, *Energy & Environmental Science*, 2019, **12**, 865-886.
2. H. J. Snaith and P. Hacke, *Nature Energy*, 2018, **3**, 459-465.
3. M. V. Khenkin, E. A. Katz, A. Abate, G. Bardizza, J. J. Berry, C. Brabec, F. Brunetti, V. Bulović, Q. Burlingame, A. Di Carlo, R. Cheacharoen, Y.-B. Cheng, A. Colsmann, S. Cros, K. Domanski, M. Dusza, C. J. Fell, S. R. Forrest, Y. Galagan, D. Di Girolamo, M. Grätzel, A. Hagfeldt, E. von Hauff, H. Hoppe, J. Kettle, H. Köbler, M. S. Leite, S. Liu, Y.-L. Loo, J. M. Luther, C.-Q. Ma, M. Madsen, M. Manceau, M. Matheron, M. McGehee, R. Meitzner, M. K. Nazeeruddin, A. F. Nogueira, Ç. Odabaşı, A. Osherov, N.-G. Park, M. O. Reese, F. De Rossi, M. Saliba, U. S. Schubert, H. J. Snaith, S. D. Stranks, W. Tress, P. A. Troshin, V. Turkovic, S. Veenstra, I. Visoly-Fisher, A. Walsh, T. Watson, H. Xie, R. Yıldırım, S. M. Zakeeruddin, K. Zhu and M. Lira-Cantu, *Nature Energy*, 2020, **5**, 35-49.
4. L. Meng, J. You and Y. Yang, *Nature Communications*, 2018, **9**, 5265.
5. A. Marronnier, G. Roma, S. Boyer-Richard, L. Pedesseau, J.-M. Jancu, Y. Bonnassieux, C. Katan, C. C. Stoumpos, M. G. Kanatzidis and J. Even, *ACS Nano*, 2018, **12**, 3477-3486.
6. J. A. Steele, H. Jin, I. Dovgaliuk, R. F. Berger, T. Braeckevelt, H. Yuan, C. Martin, E. Solano, K. Lejaeghere, S. M. J. Rogge, C. Notebaert, W. Vandezande, K. P. F. Janssen, B. Goderis, E. Debroye, Y.-K. Wang, Y. Dong, D. Ma, M. Saidaminov, H. Tan, Z. Lu, V. Dyadkin, D. Chernyshov, V. Van Speybroeck, E. H. Sargent, J. Hofkens and M. B. J. Roeffaers, *Science*, 2019, **365**, 679-684.
7. P. Becker, J. A. Márquez, J. Just, A. Al-Ashouri, C. Hages, H. Hempel, M. Jošt, S. Albrecht, R. Frahm and T. Unold, *Advanced Energy Materials*, 2019, **9**, 1900555.
8. Z. Zeng, J. Zhang, X. Gan, H. Sun, M. Shang, D. Hou, C. Lu, R. Chen, Y. Zhu and L. Han, *Advanced Energy Materials*, 2018, **8**, 1801050.
9. Q. Tai, K.-C. Tang and F. Yan, *Energy & Environmental Science*, 2019, **12**, 2375-2405.
10. Y. Han, H. Zhao, C. Duan, S. Yang, Z. Yang, Z. Liu and S. Liu, *Advanced Functional Materials*, **n/a**, 1909972.
11. W. Chen, H. Chen, G. Xu, R. Xue, S. Wang, Y. Li and Y. Li, *Joule*, 2019, **3**, 191-204.
12. K.-L. Wang, R. Wang, Z.-K. Wang, M. Li, Y. Zhang, H. Ma, L.-S. Liao and Y. Yang, *Nano Letters*, 2019, **19**, 5176-5184.
13. W. Xu, F. He, M. Zhang, P. Nie, S. Zhang, C. Zhao, R. Luo, J. Li, X. Zhang, S. Zhao, W.-D. Li, F. Kang, C.-W. Nan and G. Wei, *ACS Energy Letters*, 2019, **4**, 2491-2499.
14. Q. Wang, J. Smith A., D. Skroblin, J. Steele A., C. Wolff M., P. Caprioglio, M. Stolterfoht, H. Köbler, M. Li, S.-H. Turren-Cruz, C. Gollwitzer, D. Neher and A. Abate, *submitted*, 2020.

15. C. Liu, W. Li, H. Li, H. Wang, C. Zhang, Y. Yang, X. Gao, Q. Xue, H.-L. Yip, J. Fan, R. E. I. Schropp and Y. Mai, *Advanced Energy Materials*, 2019, **9**, 1803572.
16. H. Zhao, S. Yang, Y. Han, S. Yuan, H. Jiang, C. Duan, Z. Liu and S. Liu, *Advanced Materials Technologies*, 2019, **4**, 1900311.
17. S. Rühle, *Solar Energy*, 2016, **130**, 139-147.
18. J. Zhang, D. Bai, Z. Jin, H. Bian, K. Wang, J. Sun, Q. Wang and S. Liu, *Advanced Energy Materials*, 2018, **8**, 1703246.
19. D. H. Kim, J. H. Heo and S. H. Im, *ACS Applied Materials & Interfaces*, 2019, **11**, 19123-19131.
20. M. Stolterfoht, P. Caprioglio, C. M. Wolff, J. A. Márquez, J. Nordmann, S. Zhang, D. Rothhardt, U. Hörmann, Y. Amir, A. Redinger, L. Kegelmann, F. Zu, S. Albrecht, N. Koch, T. Kirchartz, M. Saliba, T. Unold and D. Neher, *Energy & Environmental Science*, 2019, **12**, 2778-2788.
21. C. M. Wolff, P. Caprioglio, M. Stolterfoht and D. Neher, *Advanced Materials*, 2019, **31**, 1902762.
22. P. Schulz, E. Edri, S. Kirmayer, G. Hodes, D. Cahen and A. Kahn, *Energy & Environmental Science*, 2014, **7**, 1377-1381.
23. L. E. Polander, P. Pahner, M. Schwarze, M. Saalfrank, C. Koerner and K. Leo, *APL Materials*, 2014, **2**, 081503.
24. Q. Wang, Y. Shao, Q. Dong, Z. Xiao, Y. Yuan and J. Huang, *Energy & Environmental Science*, 2014, **7**, 2359-2365.
25. C.-G. Wu, C.-H. Chiang and S. H. Chang, *Nanoscale*, 2016, **8**, 4077-4085.
26. Q. Wali, A. Fakharuddin and R. Jose, *Journal of Power Sources*, 2015, **293**, 1039-1052.
27. B. Roose, Q. Wang and A. Abate, *Advanced Energy Materials*, 2019, **9**, 1803140.
28. B. Roose, C. M. Johansen, K. Dupraz, T. Jaouen, P. Aebi, U. Steiner and A. Abate, *Journal of Materials Chemistry A*, 2018, **6**, 1850-1857.
29. Q. Jiang, L. Zhang, H. Wang, X. Yang, J. Meng, H. Liu, Z. Yin, J. Wu, X. Zhang and J. You, *Nature Energy*, 2016, **2**, 16177.
30. E. H. Anaraki, A. Kermanpur, L. Steier, K. Domanski, T. Matsui, W. Tress, M. Saliba, A. Abate, M. Grätzel, A. Hagfeldt and J.-P. Correa-Baena, *Energy & Environmental Science*, 2016, **9**, 3128-3134.
31. M. M. Tavakoli, M. Saliba, P. Yadav, P. Holzhey, A. Hagfeldt, S. M. Zakeeruddin and M. Grätzel, *Advanced Energy Materials*, 2019, **9**, 1802646.
32. S. Sanchez, N. Christoph, B. Grobety, N. Phung, U. Steiner, M. Saliba and A. Abate, *Advanced Energy Materials*, 2018, **8**, 1802060.
33. M. Stolterfoht, V. M. Le Corre, M. Feuerstein, P. Caprioglio, L. J. A. Koster and D. Neher, *ACS Energy Letters*, 2019, **4**, 2887-2892.
34. P. Caprioglio, M. Stolterfoht, C. M. Wolff, T. Unold, B. Rech, S. Albrecht and D. Neher, *Advanced Energy Materials*, 2019, **9**, 1901631.
35. U. B. Cappel, T. Daeneke and U. Bach, *Nano Letters*, 2012, **12**, 4925-4931.
36. W. H. Nguyen, C. D. Bailie, E. L. Unger and M. D. McGehee, *Journal of the American Chemical Society*, 2014, **136**, 10996-11001.
37. J. P. Correa Baena, L. Steier, W. Tress, M. Saliba, S. Neutzner, T. Matsui, F. Giordano, T. J. Jacobsson, A. R. Srimath Kandada, S. M. Zakeeruddin, A. Petrozza, A. Abate, M. K. Nazeeruddin, M. Grätzel and A. Hagfeldt, *Energy & Environmental Science*, 2015, **8**, 2928-2934.
38. J. Endres, D. A. Egger, M. Kulbak, R. A. Kerner, L. Zhao, S. H. Silver, G. Hodes, B. P. Rand, D. Cahen, L. Kronik and A. Kahn, *The Journal of Physical Chemistry Letters*, 2016, **7**, 2722-2729.
39. F. Zu, C. M. Wolff, M. Ralaiarisoa, P. Amsalem, D. Neher and N. Koch, *ACS Applied Materials & Interfaces*, 2019, **11**, 21578-21583.
40. F. Giordano, A. Abate, J. P. Correa Baena, M. Saliba, T. Matsui, S. H. Im, S. M. Zakeeruddin, M. K. Nazeeruddin, A. Hagfeldt and M. Graetzel, *Nature Communications*, 2016, **7**, 10379.
41. B. Roose and R. H. Friend, *Advanced Materials Interfaces*, 2019, **6**, 1801788.
42. Z. Yang, *Thesis*, 2018.
43. Z. Yang, A. Surrente, K. Galkowski, A. Miyata, O. Portugall, R. J. Sutton, A. A. Haghighirad, H. J. Snaith, D. K. Maude, P. Plochocka and R. J. Nicholas, *ACS Energy Letters*, 2017, **2**, 1621-1627.

44. Q. Zeng, X. Zhang, C. Liu, T. Feng, Z. Chen, W. Zhang, W. Zheng, H. Zhang and B. Yang, *Solar RRL*, 2019, **3**, 1800239.
45. H. Chung, S. I. Jung, H. J. Kim, W. Cha, E. Sim, D. Kim, W.-K. Koh and J. Kim, *Angewandte Chemie International Edition*, 2017, **56**, 4160-4164.
46. J. Yang, X. Wen, H. Xia, R. Sheng, Q. Ma, J. Kim, P. Tapping, T. Harada, T. W. Kee, F. Huang, Y.-B. Cheng, M. Green, A. Ho-Baillie, S. Huang, S. Shrestha, R. Patterson and G. Conibeer, *Nature Communications*, 2017, **8**, 14120.
47. S. A. Bretschneider, F. Laquai and M. Bonn, *The Journal of Physical Chemistry C*, 2017, **121**, 11201-11206.
48. J. Fu, Q. Xu, G. Han, B. Wu, C. H. A. Huan, M. L. Leek and T. C. Sum, *Nature Communications*, 2017, **8**, 1300.
49. A. K. Chandiran, F. Sauvage, M. Casas-Cabanas, P. Comte, S. M. Zakeeruddin and M. Graetzel, *The Journal of Physical Chemistry C*, 2010, **114**, 15849-15856.
50. B. Roose, K. C. Gödel, S. Pathak, A. Sadhanala, J. P. C. Baena, B. D. Wilts, H. J. Snaith, U. Wiesner, M. Grätzel, U. Steiner and A. Abate, *Advanced Energy Materials*, 2016, **6**, 1501868.
51. B. Roose, S. Pathak and U. Steiner, *Chemical Society Reviews*, 2015, **44**, 8326-8349.
52. A. Gagliardi and A. Abate, *ACS Energy Letters*, 2018, **3**, 163-169.
53. C. M. Wolff, L. Canil, C. Rehermann, N. Ngoc Linh, F. Zu, M. Ralaiarisoa, P. Caprioglio, L. Fiedler, M. Stolterfoht, S. Kogikoski, I. Bald, N. Koch, E. L. Unger, T. Dittrich, A. Abate and D. Neher, *ACS Nano*, 2020, **14**, 1445-1456.
54. M. A. Ruiz-Preciado, D. J. Kubicki, A. Hofstetter, L. McGovern, M. H. Futscher, A. Ummadisingu, R. Gershoni-Poranne, S. M. Zakeeruddin, B. Ehrler, L. Emsley, J. V. Milić and M. Grätzel, *Journal of the American Chemical Society*, 2020, **142**, 1645-1654.